

Formation of high entropy metal diborides using arc-melting and combinatorial approach to study quinary and quaternary solid solutions

Original

Formation of high entropy metal diborides using arc-melting and combinatorial approach to study quinary and quaternary solid solutions / Failla, S.; Galizia, P.; Fu, S.; Grasso, S.; Sciti, D.. - In: JOURNAL OF THE EUROPEAN CERAMIC SOCIETY. - ISSN 0955-2219. - ELETTRONICO. - 40:3(2020), pp. 588-593. [10.1016/j.jeurceramsoc.2019.10.051]

Availability:

This version is available at: 11583/2952097 since: 2022-01-21T14:05:38Z

Publisher:

Elsevier Ltd

Published

DOI:10.1016/j.jeurceramsoc.2019.10.051

Terms of use:

This article is made available under terms and conditions as specified in the corresponding bibliographic description in the repository

Publisher copyright

Elsevier postprint/Author's Accepted Manuscript

© 2020. This manuscript version is made available under the CC-BY-NC-ND 4.0 license
<http://creativecommons.org/licenses/by-nc-nd/4.0/>. The final authenticated version is available online at:
<http://dx.doi.org/10.1016/j.jeurceramsoc.2019.10.051>

(Article begins on next page)

Formation of high entropy metal diborides using arc-melting and combinatorial approach to study quinary and quaternary solid solutions

Simone Failla^{a}, Pietro Galizia^a, Shuai Fu^b, Salvatore Grasso^{b*}, Diletta Sciti^a*

^a CNR-ISTEC, National Research Council of Italy - Institute of Science and Technology for Ceramics, Via Granarolo 64, 48018, Faenza, Italy

^b Key Laboratory of Advanced Technologies of Materials, Ministry of Education, School of Materials Science and Engineering, Southwest Jiaotong University, Chengdu 610031, China

*Corresponding authors:

Simone Failla, National Research Council of Italy - Institute of Science and Technology for Ceramics (CNR-ISTEC), Via Granarolo 64, 48018, Faenza, Italy, Tel: +39 0546 699 723, E-mail addresses: simone.failla@istec.cnr.it

Prof. Salvatore Grasso, School of Materials Science and Engineering Southwest Jiaotong University Chengdu, Sichuan, 610031, China, Tel/Fax: +68 28 8760 0454, E-mail: s.grasso@swjtu.edu.cn

Keywords: Arc-melting, High entropy metal diborides, Hardness, Microstructure, X-ray diffraction

Abstract

High entropy metal diborides (HEBs) represent a radically new approach to extend the chemical composition window of ultra-high temperature ceramics (UHTCs). In this work, arc-melting was used to produce dense HEBs starting from UHTC powders. In order to understand the influence of each individual diboride within the quinary system (HfB₂, ZrB₂, TiB₂, TaB₂ and CrB₂), we investigated five quaternary equimolar solid solutions *e.g.* Hf-Zr-Ti-Ta, Hf-Zr-Ti-Cr, Hf-Zr-Ta-Cr, Hf-Ti-Ta-Cr, Zr-Ti-Ta-Cr and the overall quinary equimolar combination. Arc-melting allowed a rapid screening of favorable and unfavorable combinations. The produced HEBs were free from undesired oxides and characterized by linear variation of lattice parameters typical of diborides and binary solid solutions. Because of evaporation during arc melting, CrB₂ was hardly found in the solid solution, suggesting that vapor pressure should be taken into account when designing HEB

1 compositions especially for operating temperatures exceeding 2000 °C. Finally, Vickers
2 microhardness ranged between the typical values of starting diborides.
3
4
5
6
7

8 **1. Introduction**

9

10 Borides and carbides of transition metals such as, ZrB₂, TiB₂, HfC, TaC, are known as ultra-
11 high temperature ceramics (UHTCs). Owing to their particularly chemical and physical properties,
12 high melting temperatures above ~3000 °C, excellent high temperature strengths, high hardness,
13 good thermal and electrical conductivity and ablation resistance [1], UHTCs can be used in extreme
14 temperatures and chemically aggressive environments. UHTCs are difficult to densify because of
15 their melting point higher than 3000°C resulting from strong covalent bonding [1,2]. Current UHTC
16 applications in hypersonic flights and rocket propulsion have operation requirements exceeding
17 bulk mono-phasic materials. Pure monolithic ceramics present a series of limitations, such as poor
18 damage tolerance and critical oxidation resistance [3,4]. Several studies have demonstrated that
19 combining UHTCs with other elements such as metals [5], carbides, borides, nitrides [6] and metal
20 disilicides [7], can help to solve some of these major drawbacks.
21
22
23
24
25
26
27
28
29
30
31
32
33
34
35
36
37
38
39
40

41 In recent years, high entropy alloys (HEA) have attracted growing interest [8–10]. Starting
42 from work on metals, these new alloys are composed of “*r*”-number of metal specimens, generally
43 $r \geq 5$, to form a high entropy solution having increased entropy of mixing
44
45 $\Delta S_{mix} = -nR \sum_{i=1}^r x_i \ln x_i$, where n is the total number of moles, R is the gas constant, x_i is the mole
46 fraction of component i [9]. The theory supporting these new alloys relies upon the principle of
47 Gibbs free energy minimization, $\Delta G = \Delta H - T \cdot \Delta S$. According to this principle, a system with an
48 enhanced entropy (ΔS) is more stable ($\Delta G < 0$) at high temperatures thanks to the contribution of the
49 entropic term ($-T \cdot \Delta S$). HEAs have been shown to have improved properties compared to
50 conventional alloys. Further necessary conditions for the existence of the substitutional solid
51
52
53
54
55
56
57
58
59
60
61
62
63
64
65

1 solutions are set by the Hume-Rothery solid solution rules. Indeed, in order to obtain substitute
2 alloys, two or more metals must meet the following requirements: 1) atomic radii that do not differ
3 by more than 15 %, 2) same crystal structure, 3) similar electronegativity, 4) same valence.
4
5

6
7 High entropy oxides [11–14], borides [15–19], carbides [20–23] and silicides [24] have been
8 obtained using different synthesis/sintering techniques such as spark plasma sintering and
9 pressureless sintering. For instance, Gild et al. [13] have successfully synthesized high-entropy
10 fluorite oxides (HEFO), with hardness comparable to 8 mol. Y₂O₃-stabilized ZrO₂ and low
11 electrical and thermal conductivities. Castel et al. [21] have shown a significant enhancement in
12 hardness of high entropy carbides material compared to the value calculated according to the rule of
13 mixtures from the reference monocarbides and in comparison to the hardest monocarbide. Tallarita
14 et al. [17] have produced high entropy borides starting from the respective oxides and boron,
15 through a two-step processing method of Self-propagating High-temperature Synthesis (SHS)
16 followed by SPS. This approach avoided the need for intense mechanical milling of individual
17 borides. Although reactive sintering by SPS may be faster than hot pressing and pressureless
18 sintering, it still requires costly equipment, high temperatures (>2000 °C) and high pressures (tens
19 of MPa) to promote atomic diffusion of different elements to obtain solid solutions. Alternatively,
20 Zhang et al. [25] have obtained solid solutions of binary and ternary carbides in a very short time
21 (10-20 seconds) using the arc melting technique. This technique, already known in the metallurgical
22 field, is able to reach very high temperatures, and therefore, melting materials with high melting
23 point, close to 4000 °C, in a short time (a few seconds). In this way it was possible demonstrate the
24 formation of solid solutions of binary, ternary carbides.
25
26
27
28
29
30
31
32
33
34
35
36
37
38
39
40
41
42
43
44
45
46
47
48
49

50 The aim of this work is to demonstrate the feasibility of high entropy borides (HEB), mixing
51 equimolar composition of HfB₂, ZrB₂, TiB₂, TaB₂ and CrB₂, through the arc-melting technique.
52 Moreover, since this technique allows rapid fabrication of large number of samples, we prepared 6
53 compositions (one quinary and five quaternaries) to study the effect of each single boride on the
54 formation of HEB solid solutions.
55
56
57
58
59
60
61

2. Experimental

Five commercial powders of transition metal diborides of HfB₂ (Treibacher, D₅₀ 2.56 μm, impurities (wt.%): 0.23 C, 0.01 N, 0.23 O, <0.001 S), TaB₂ (Materion, purity 99.5%, impurities (wt.%): 0.04 Al, < 0.0007 Cd, < 0.0005 Cr, 0.07 Fe, 0.02 Nb, <0.0004 Pb), TiB₂ (H.C. Starck, Grade F, D₉₀ 4.0 -7.0 μm, D₅₀ 2.5-3.5 μm, impurities (wt. %): 0.4 C, 2.5 O, 0.5 N, 0.1 Fe), ZrB₂ (H.C. Starck, Grade B, D₉₀ 4.0 -6.0 μm, D₅₀ 1.5-3 μm, impurities (wt. %): 0.2 C, 1.5 O, 0.25 N, 0.1 Fe, 0.2 Hf), CrB₂ (H.C. Starck, Grade B, D₉₀ 4.0 -6.0 μm, D₅₀ 1.5-3 μm, impurities (wt. %): 0.3 C, 0.6 O, 0.5 Fe) were used to prepare six mixtures. One with all five equimolar elements and five equimolar combinations of 4 out of 5 borides: e.g (HfB₂, ZrB₂, TiB₂, TaB₂), (HfB₂, ZrB₂, TiB₂, CrB₂) (HfB₂, ZrB₂, CrB₂, TaB₂), (HfB₂, CrB₂, TiB₂, TaB₂), (CrB₂, ZrB₂, TiB₂, TaB₂). The six compositions are listed in Table 1. The starting equimolar powders were mixed **using mortar and pestle and rotary milled with no milling media**. All mixtures were **pre-sintered in a** Spark plasma sintering furnace (Chenhua 10–20 SPS furnace, China), at 1600 °C **in low vacuum (5 Pa)** under a pressure of 25 MPa, heating rate of 80 °C/min and dwelling time of 10 minutes, in order to clean borides from oxide impurities as much as possible. From each of the 6 pre-sintered pellets, 10 smaller pieces with a volume of about 40 mm³ were obtained for the arc-melting experiments in order to have similar heating and cooling rates.

All samples were melted on a water-cooled copper crucible using arc melting by TIG-200P (AC/DC) (Dongguan Hanhuang Welding and Cutting Equipment Co., Ltd, China) under argon flow, with purity of 99.999 %, applying a current of 100 A for 10-20 seconds. The argon flow was maintained for 10 seconds after switching off the current in order to protect the samples from the oxidation during the free cooling. The samples were re-melted 5 times in order to homogenize the mixture **as much as possible** during **melt** formation.

Bulk densities were measured by the Archimede method, using ethyl alcohol instead of water. Several specimens were measured for each composition and the results were averaged. The microstructure was analyzed on polished cross sections, using diamond discs up to 0.25 μm , by field-emission scanning electron microscopy (FESEM, mod. SIGMA, ZEISS NTS GmbH, Oberkochen, Germany) equipped with energy X-ray dispersive microanalysis (EDS, Model INCA energy 300; Oxford Instruments, UK). Crystalline phases of the samples, obtained from the melt, were identified by X-ray diffraction (XRD, mod. D8 Advance - Bruker, Germany) with Cu $K\alpha$ radiation, step size of 0.04 and 0.5 s counting rate in the 20–100° 2 θ range. The hardness was measured by Vickers indentation method applying a load of 1.96 N (200 g), 4.90 N (500 g) and 9.8 N (1000 g) (Innovatest Falcon 505, Rupac, Netherlands) for 15 seconds.

Table 1. Starting compositions, density values, and quantitative EDS mapping of samples core

Label	Starting composition mol%	Bulk density g/cm ³	EDS analysis*				
			Hf	Zr	Ti	Ta	Cr
1 - all	(Hf _{0.20} , Zr _{0.20} , Ti _{0.20} , Ta _{0.20} , Cr _{0.20})B ₂	7.9 ± 0.2	25	22	23	27	1
2 - CrB ₂	(Hf _{0.25} , Zr _{0.25} , Ti _{0.25} , Ta _{0.25})B ₂	9.3 ± 0.5	27	24	22	25	-
3 - TaB ₂	(Hf _{0.25} , Zr _{0.25} , Ti _{0.25} , Cr _{0.25})B ₂	6.9 ± 0.2	39	30	30	-	1
4 - TiB ₂	(Hf _{0.25} , Zr _{0.25} , Cr _{0.25} , Ta _{0.25})B ₂	9.4 ± 0.2	32	30	-	36	0.8
5 - ZrB ₂	(Hf _{0.25} , Cr _{0.25} , Ti _{0.25} , Ta _{0.25})B ₂	8.5 ± 0.2	37	-	29	31	2
6 - HfB ₂	(Cr _{0.25} , Zr _{0.25} , Ti _{0.25} , Ta _{0.25})B ₂	5.6 ± 0.4	-	33	32	33	1

*error within 3% measured using EDS

3. Results and discussion

3.1 X-ray diffraction spectra.

Fig. 1 shows X-ray diffraction spectra: all samples display the primitive hexagonal unit cell typical of the isomorphous starting diborides. Principal diffractions are usually surrounded by small peaks (< 2% of highest peak, see bottom enlarged spectra below each diffraction pattern), which accounts for phase separation, as discussed in sections 3.2 and 3.4.

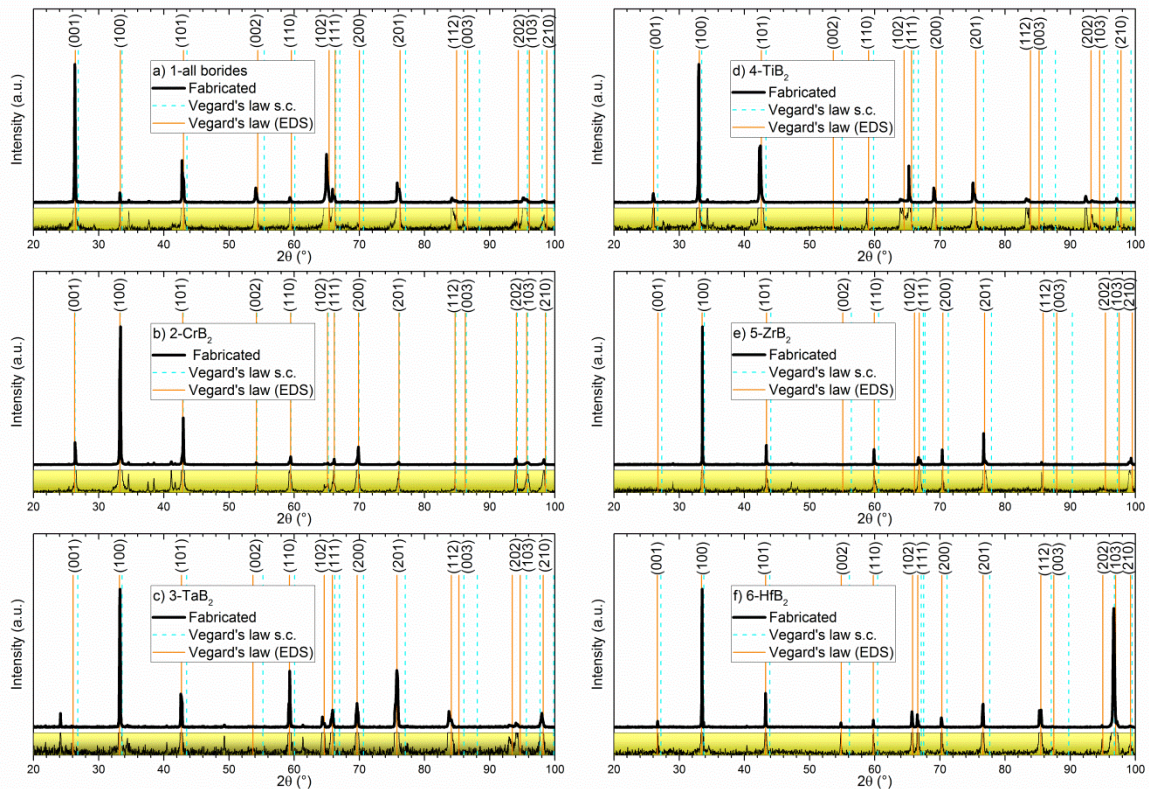


Figure 1: Normalized X-ray diffraction patterns for the 6 mixtures and expected peaks' position of high entropy metal diborides (HEBs) calculated with the Vegard's law considering the starting compositions (s.c.) and the compositions detected by EDS. All scales of the insets zoom range from 0 to 0.02.

Nevertheless, considering main peaks ascribed to hexagonal phase, experimental lattice parameters obtained from XRD patterns are shown in Table 2 together with those calculated by means of Vegard's rule [26]. The calculation was done using powder diffraction files (PDF) n. 65-0878, 65-1073, 65-1883, 65-3389, and 65-3387 for TaB₂, TiB₂, CrB₂, HfB₂, ZrB₂, respectively, and the actual atomic percentage obtained using EDS analysis explained below. As it can be seen from Fig. 1, the deviation from Vegard's rule is minimized if compositions determined by EDS analysis are taken into account instead of the starting equimolar ones. In Fig. 2 we plotted a series of observed lattice parameters of various diborides and binary solid solutions taken from Ref. [27], along with those of the HEBs solutions developed in this work. As can be seen, there is an excellent agreement

between a linear interpolation of observed c/a ratio vs. atomic radii of metal atom, r_m and the plotted values, the only unexpected outlier is 3-TaB₂.

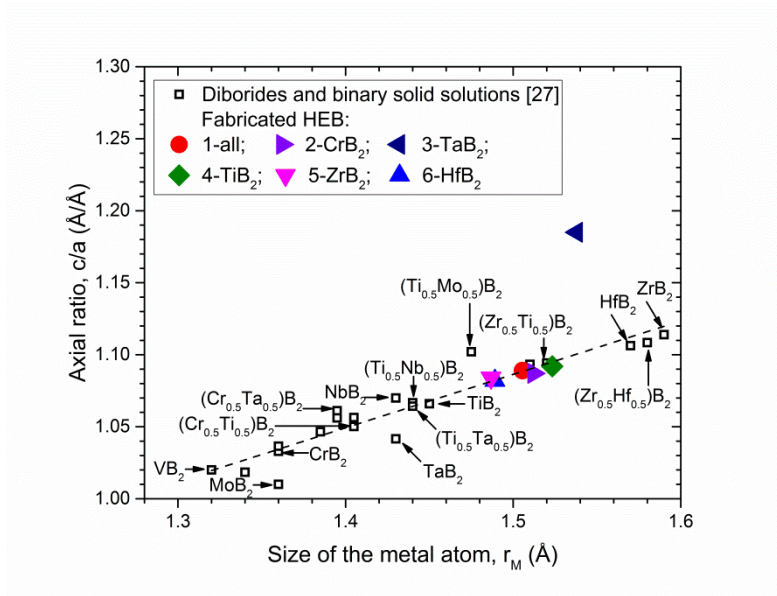


Figure 2: Observed tetragonality, c/a ratio, vs. atomic radii of metal atom, r_m , for diborides and binary solid solutions taken from Ref. [27], along with those of the high entropy metal diborides (HEBs) developed in this work. The dotted line was obtained by linear fitting ($R^2 = 0.90$) the values of diborides and binary solid solutions.

The reason for the large deviation (8%) in the length of the c -axis is not known, and to date, such anomalies were observed in other studies as well [27] but no explanation has been found so far. In summary, XRD results suggest that (i) there is a negligible or no amount of Cr in solid solution, and (ii) metal-to-metal replacement to form solid solution occurred readily in the Hf, Zr, Ti, and Ta diborides.

Table 2. Lattice constants a , and c (Å) obtained from observed (100) and (001) peaks, respectively, compared to the one calculated using Vegard's rule and the actual atomic percentage obtained using EDS analysis. c values of sample 5 were extrapolated from (101) peak.

	a XRD	a Vegard	c XRD	c Vegard	c/a XRD	c/a Vegard
1- all	3.109	3.102	3.387	3.370	1.089	1.086
2-CrB ₂	3.101	3.107	3.372	3.382	1.087	1.089
3-TaB ₂	3.107	3.115	3.683	3.413	1.185	1.096
4-TiB ₂	3.132	3.125	3.421	3.415	1.092	1.093
5-ZrB ₂	3.082	3.085	3.340	3.330	1.084	1.080
6-HfB ₂	3.086	3.091	3.338	3.344	1.082	1.082

3.2 Sample morphology and EDS analysis

Fig. 3 shows the cross section of the samples obtained from the arc-melting process of the six materials listed in Table 1. From SEM analyses of the microstructures it was ascertained that all materials reached a good level of densification, with the exception of 4-TiB₂, (missing TiB₂) that exhibited small distributed porosity in the center and voids in the edges (see supplementary section). Bulk densities measured with the Archimede method (Table 2) ranges from 5.6 to 9.4 g/cm³, depending on the composition and residual porosity. Due to evaporation phenomena and new phase formation during arc-melting (section 3.4), the starting composition was strongly modified, therefore an exact calculation of theoretical and relative densities was not possible.

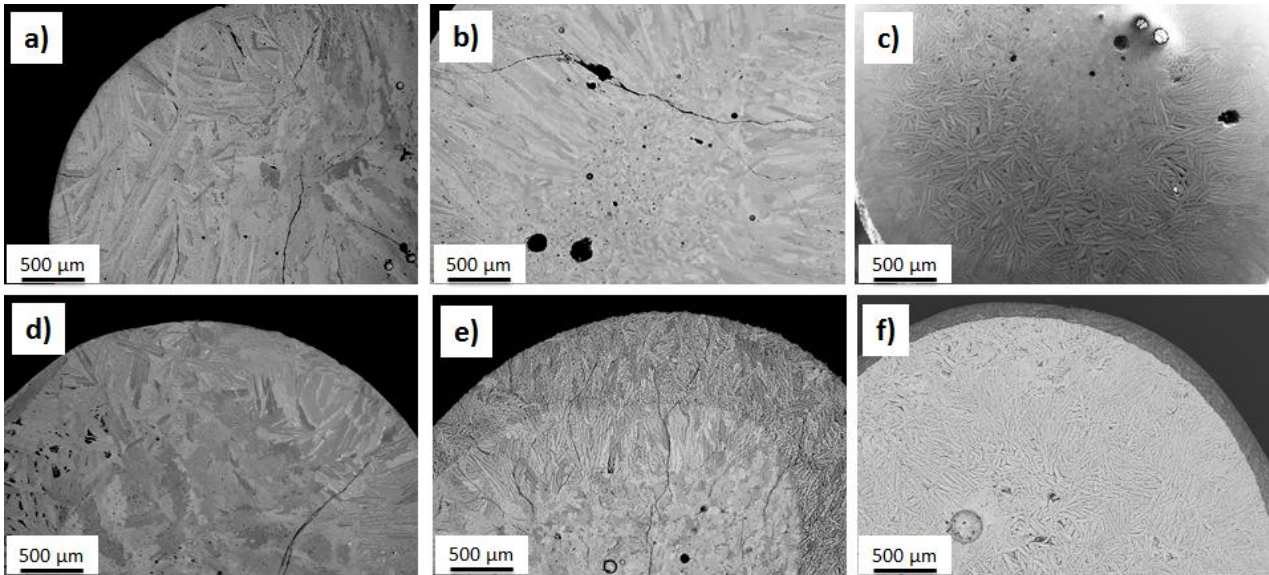


Figure 3. Cross section of spherical HEB samples:

a) 1- all, b) 2- CrB₂, c) 3- TaB₂, d) 4-TiB₂, e) 5- ZrB₂, f) 6- HfB₂.

Dense specimens were often found to be affected by cracks due to thermal shock/strong temperature gradient experienced during arc-melting treatment. They all exhibited the typical anisotropic microstructure of metallic materials obtained from melting [28,29]. During cooling down, the surface cooled much faster than the core, which generated a strong radial temperature gradient. As a result, an anisotropic structure was created, with rounded/coarsened grains in the (hot) core that gradually changed to elongated and dendritic-like grains towards the rapidly cooling surface.

Approximately, the transition from rounded to elongated grains occurred at a distance of 2 mm from the center. According to EDS analyses, a single solid solution phase was detected in the core grains constituting the inner part of the molten samples, in agreement with the phases detected by X-ray diffraction and in agreement with the large mutual solubility range of diborides observed by other authors [30]. Moreover, grain boundaries were found to be clean in this portion of material, at least at SEM resolution. Shifting from the core to the edge, compositions and morphology of the grains changed and liquid phase separation was observed in the grain boundary regions.

In all the compositions containing Cr, this element was preferentially detected along the grain boundaries as a secondary phase, though a tiny percentage was also found in solid solution (see

1
2
3
4
5
6
7
8
9
10
11
12
13
14
15
16
17
18
19
20
21
22
23
24
25
26
27
28
29
30
31
32
33
34
35
36
37
38
39
40
41
42
43
44
45
46
47
48
49
50
51
52
53
54
55
56
57
58
59
60
61
62
63
64
65

quantitative analyses in Table 1). Indeed, observing the EDS compositional maps of sample 1-all ($\text{Hf}_{0.20}, \text{Zr}_{0.20}, \text{Ti}_{0.20}, \text{Ta}_{0.20}, \text{Cr}_{0.20}$) B_2 , Fig. 4, and except those contain Cr, they presented a quasi-equimolar solid solution of HfB_2 , ZrB_2 , TiB_2 and TaB_2 . This feature is even more evident in sample 2- CrB_2 where CrB_2 was not included the original mixture.

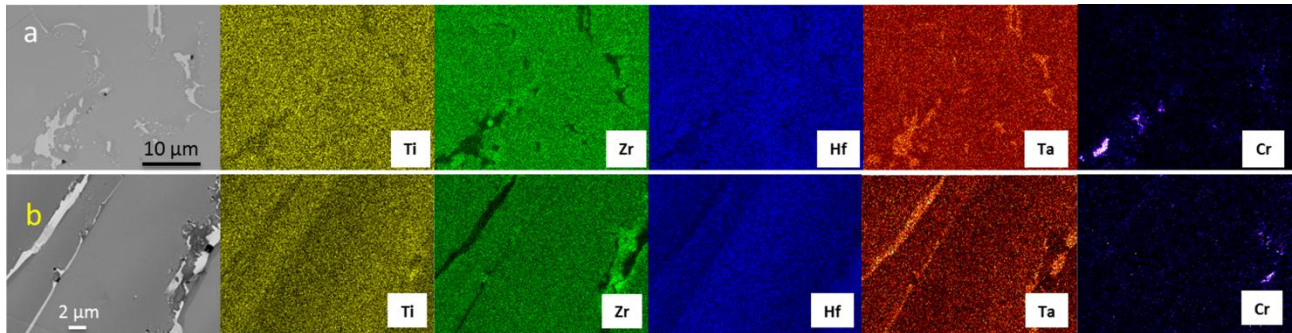


Figure 4. EDS compositional maps of a) inner part and b) external part of the sample 1-all b, containing all borides. CrB_2 phase separation was observed, the remaining borides formed a complete solid solution

Noteworthy, in sample 2- CrB_2 ($\text{Hf}_{0.25}, \text{Zr}_{0.25}, \text{Ti}_{0.25}, \text{Ta}_{0.25}$) B_2 , missing Cr, Ta segregation between the grains was observed, as shown in Fig 5 b)..

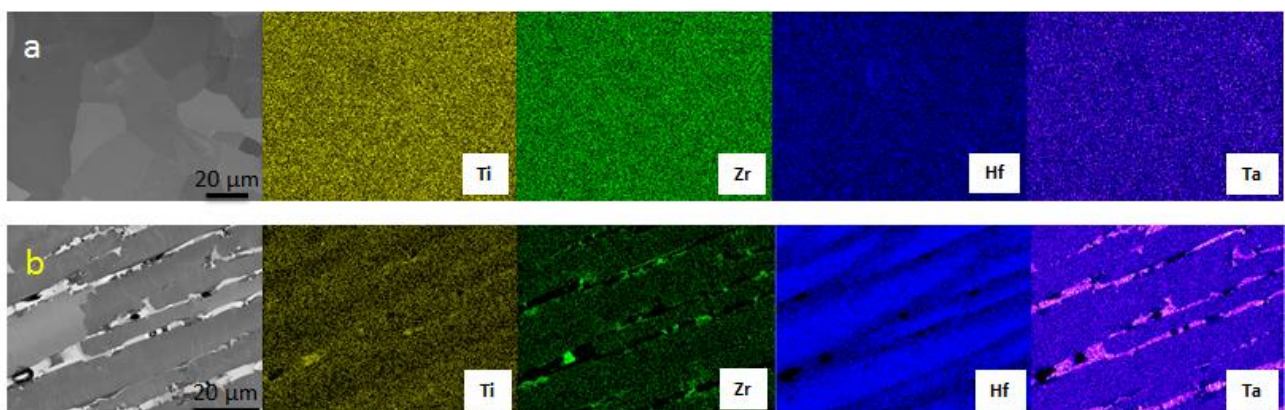


Figure 5. EDS compositional maps of a) inner part and b) external part of the sample 2- CrB_2 .

1 For mixtures 3, 4, 5 and 6, figures are reported in the supplementary material. Sample 3, (Hf_{0.25},
2 Zr_{0.25}, Ti_{0.25}, Cr_{0.25})B₂, was characterized by a solid solution with almost equal atomic content of Hf,
3 Zr, and Ti, but much smaller content of Cr. Cr was preferentially detected at the grain boundaries.
4
5 Towards the edge of the pellet, we noticed that elongated grains composed of Hf, Zr, and Ti were
6
7 surrounded by ZrB₂ rounded agglomerates and CrB₂ phases (see Fig. A1 a) and b)).
8
9 Similarly, sample 4 (Hf_{0.25}, Zr_{0.25}, Cr_{0.25}, Ta_{0.25})B₂, displayed **homogeneous distribution of Zr, Hf**
10 **and Ta element** in the center **grains**, with small **segregated** CrB₂ – based secondary phases **at the**
11 **grain boundaries** On the contrary, going towards the edge, elongated grains were surrounded by
12 mixed **secondary** phase with irregular morphology (see Fig. A2 a) and b)) containing
13 **inhomogeneous distribution of Zr, Hf, Ta mainly and Cr in small quantities**. Samples 5 (Hf_{0.25},
14 Cr_{0.25}, Ti_{0.25}, Ta_{0.25})B₂ and 6 (Cr_{0.25}, Zr_{0.25}, Ti_{0.25}, Ta_{0.25})B₂, showed characteristics **similar to sample**
15 **4** (see Fig. A3 a) and b) and A4 a) and b)).
16
17
18
19
20
21
22
23
24
25
26
27
28
29
30
31

32 *3.3 Hardness*

33
34
35 Indentations were collected indistinctly **both** in the **samples core** and close to the sample surface.
36
37 Values were in the range 19-20 GPa, and slightly increased to 20-23 GPa reducing the load from 1
38 to 0.5 and 0.2 Kg, **as** shown in Fig. 6 and Table 2A, mainly due to the indentation size effect [31],
39
40
41
42
43 [32].
44
45
46
47
48
49
50
51
52
53
54
55
56
57
58
59
60
61
62
63
64
65

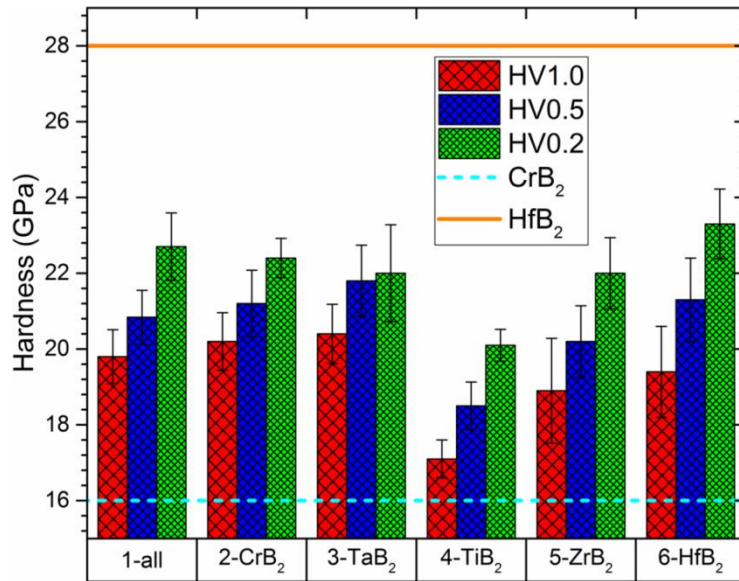


Figure 6. Hardness value measured with load 1, 0.5 and 0.2 Kg for quaternary and quinary borides. HfB₂ and CrB₂ lines are the hardest and softest borides as reference materials such as indicated by Fahrenholtz et al. (HV1.0) [1] and Wang et al. (HV0.5) [33]

The lowest values were found for the mixture without TiB₂, a feature which can be attributed to residual porosity shown in figure 3 d). Amongst the other fully dense mixtures, the hardest one was sample 3, missing TaB₂ probably due to its finer microstructure. Table 1A shows physical and chemical properties of the transition metal diborides considered in this work. They all satisfy the Hume-Rothery solid solution rule, as demonstrated by [15].

3.4 Microstructural evolution

In their work, Gild et al. [15], demonstrated the formation of a high entropy phase including CrB₂ using the spark plasma sintering technique, despite the limited solid solubility of CrB₂ in both HfB₂ and ZrB₂ [27]. In our case, the formation of high entropy diboride should be easier because, in the molten state, the activation energy for diffusion is much smaller than in the solid state [34].

Compared to the starting compositions we observed a notable reduction of CrB₂ content in all mixtures and of TaB₂ in the case of 2-CrB₂, (e.g. the mixture missing CrB₂). Indeed, we

1 hypothesized that in the arc melting process, formation of solid solutions is not **only** affected by
2 melting points of each **constituent** material, but also by **their** vapor partial pressure. In this work,
3
4 CrB₂ has the highest vapor partial pressure followed by TaB₂, **as** shown in Table 1A.. Therefore, in
5
6 samples containing CrB₂ (1, 3, 4, 5, 6) the peculiar microstructure obtained is affected by the fast
7
8 vaporization and evaporation of CrB₂ from the center towards the surface. To a lower extent, TaB₂
9
10 also experienced the same phenomenon, because of its high vapor partial pressure. Broadly,
11
12 microstructural evolution of compositions containing CrB₂ can be schematized as follows. During
13
14 heating:
15
16

- 17 1) at least 2 melts form, with different melting points and composition. Since CrB₂ melting point <<
18
19 other borides, at temperature around 2000°C or below CrB₂ becomes liquid and partially dissolves
20
21 other borides in the vicinity, forming the L1 liquid phase.
22
23
- 24 2) As the temperature continues to rise and melting proceeds towards the pellet interior, new L1 liquid
25
26 phase is formed and evaporation of CrB₂ occurs on the surface.
27
28
- 29 3) Other molten liquids form (L2, with no CrB₂), with higher melting point than L1.
30
31
- 32 4) Progressive/fast extension of melting from the surface down to the core and progressive depletion
33
34 of CrB₂ from the core.
35
36

37 During cooling:

- 38 1) the solid solution nuclei from L2 (most refractory) liquid type begin to solidify from the outer
39
40 surface and grow forming columnar grains that develop in the direction of the temperature gradient
41
42 present in the sample. These crystalline nuclei are mainly formed by solid solutions of the high
43
44 melting elements, where HfB₂, ZrB₂, TiB₂ are quasi equimolar whilst TaB₂ is slightly lower due to
45
46 partial evaporation.
47
48
- 49 2) CrB₂ vaporization is blocked in the proximity of the outer surface due to rapid closure of exit
50
51 channels and the CrB₂-liquid phase (L1) remains trapped and solidifies along the grain boundaries,
52
53
54
55
56
57
58 as observed by SEM-EDS.
59
60
61
62
63
64
65

3) CrB₂ secondary melt separation occurs because of different factors, including its reduced melting point compared to other borides, decreased solubility of other borides when the temperature decreases and extremely fast cooling (≈ 1000 °C/s).

Finally, in sample 2, missing CrB₂, TaB₂ is the lowest melting temperature phase, thus in this case, TaB₂ based liquid phase is formed and phase separation mainly involving TaB₂ occurs during cooling.

Mechanisms occurring during cooling are sketched in Fig. 7.

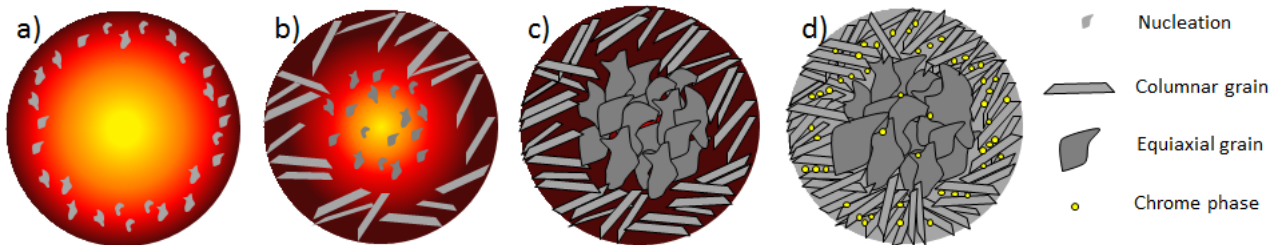


Figure 7. Solidification mechanism: a) first formation of crystalline nuclei in the outermost area formed by the high melting elements (HfB₂, ZrB₂, TiB₂, TaB₂), b) nuclei growth forming columnar grains that develop in the direction of the temperature gradient and formation of crystalline nuclei in the central part of the sample c) growth of the equiaxial grains in the innermost area of the material formed by an equimolar solid solution d) precipitation of Cr element among the grain boundary principally in the external part of the sample

Finally, future work is concerned with additional experiments to control the cooling rate. It is expected that producing larger samples has the effect to decrease the cooling rate, limiting or suppressing the formation of a core – shell structure, with the dense equiaxed core and elongated shell grains. This could be achieved by lowering the arc current **gradually** or using a heated stage.

4. Conclusions

High entropy metal diborides were obtained using the arc-melting technique starting from a powder mixture. HfB₂, ZrB₂, TiB₂ and TaB₂ formed equimolar solid solutions as confirmed by EDS analysis. Unlike solid state processing, the similarity in melting point and vapor partial pressure of each individual diboride is an essential requirement to achieve homogenous samples using arc-melting technique. CrB₂ did not form a solid solution because during processing its low melting point contributed to phase separation while its high vapor partial pressure induced almost complete sublimation. The XRD analysis confirmed that oxide phases were not present and the values of lattice parameters were in agreement with theoretical values. The influence of each element on the hardness values showed no large variations and lowest value was for the sample without TiB₂. The results obtained in this work demonstrates as arc-melting technique could allow a rapid screening of hundreds of high entropy borides compositions avoiding long reaction times needed in solid state processing.

Acknowledgments

The authors would like to thank M. Mazzocchi (ISTEC-CNR, Italy) for recording XRD spectra. This research did not receive any specific grant from funding agencies in the public, commercial, or not-for-profit sectors. SG was supported by Thousand Talents Program of China and Sichuan Province.

References

- [1] W.G. Fahrenholtz, G.E. Hilmas, I.G. Talmy, J.A. Zaykoski, Refractory diborides of zirconium and hafnium, *J. Am. Ceram. Soc.* 90 (2007) 1347–1364. doi:10.1111/j.1551-2916.2007.01583.x.
- [2] J.K. Sonber, A.K. Suri, Synthesis and consolidation of zirconium diboride: review, *Adv. Appl. Ceram.* 110 (2011) 321–334. doi:10.1179/1743676111y.0000000008.
- [3] T.A. Parthasarathy, R.A. Rapp, M. Opeka, R.J. Kerans, A Model for Transitions in Oxidation Regimes of ZrB_2 , *Mater. Sci. Forum.* 595–598 (2008) 823–832. doi:10.4028/www.scientific.net/MSF.595-598.823.
- [4] T.A. Parthasarathy, R.A. Rapp, M. Opeka, R.J. Kerans, A model for the oxidation of ZrB_2 , HfB_2 and TiB_2 , *Acta Mater.* 55 (2007) 5999–6010. doi:10.1016/j.actamat.2007.07.027.
- [5] H. Wang, D. Chen, C.A. Wang, R. Zhang, D. Fang, Preparation and characterization of high-toughness ZrB_2 /Mo composites by hot-pressing process, *Int. J. Refract. Met. Hard Mater.* 27 (2009) 1024–1026. doi:10.1016/j.ijrmhm.2009.06.003.
- [6] F. Monteverde, A. Bellosi, S. Guicciardi, Processing and properties of zirconium diboride-based composites, *J. Eur. Ceram. Soc.* 22 (2002) 279–288. doi:10.1016/S0955-2219(01)00284-9.
- [7] L. Silvestroni, S. Failla, I. Neshpor, O. Grigoriev, Method to improve the oxidation resistance of ZrB_2 -based ceramics for reusable space systems, *J. Eur. Ceram. Soc.* 38 (2018) 2467–2476. doi:10.1016/j.jeurceramsoc.2018.01.025.
- [8] J.W. Yeh, S.K. Chen, S.J. Lin, J.Y. Gan, T.S. Chin, T.T. Shun, C.H. Tsau, S.Y. Chang, Nanostructured high-entropy alloys with multiple principal elements: Novel alloy design concepts and outcomes, *Adv. Eng. Mater.* 6 (2004) 299-303+274.

doi:10.1002/adem.200300567.

- 1
2
3 [9] Y. Zhang, T.T. Zuo, Z. Tang, M.C. Gao, K.A. Dahmen, P.K. Liaw, Z.P. Lu, Microstructures
4 and properties of high-entropy alloys, *Prog. Mater. Sci.* 61 (2014) 1–93.
5
6 doi:10.1016/j.pmatsci.2013.10.001.
7
8
9
10
11 [10] M.H. Tsai, J.W. Yeh, High-entropy alloys: A critical review, *Mater. Res. Lett.* 2 (2014) 107–
12 123. doi:10.1080/21663831.2014.912690.
13
14
15
16
17 [11] C.M. Rost, E. Sachet, T. Borman, A. Moballegh, E.C. Dickey, D. Hou, J.L. Jones, S.
18 Curtarolo, J.P. Maria, Entropy-stabilized oxides, *Nat. Commun.* 6 (2015) 1–8.
19
20 doi:10.1038/ncomms9485.
21
22
23
24
25 [12] S. Jiang, T. Hu, J. Gild, N. Zhou, J. Nie, M. Qin, T. Harrington, K. Vecchio, J. Luo, A new
26 class of high-entropy perovskite oxides, *Scr. Mater.* 142 (2018) 116–120.
27
28 doi:10.1016/j.scriptamat.2017.08.040.
29
30
31
32
33 [13] J. Gild, M. Samiee, J.L. Braun, T. Harrington, H. Vega, P.E. Hopkins, K. Vecchio, J. Luo,
34 High-entropy fluorite oxides, *J. Eur. Ceram. Soc.* 38 (2018) 3578–3584.
35
36 doi:10.1016/j.jeurceramsoc.2018.04.010.
37
38
39
40
41 [14] M. Biesuz, S. Fu, J. Dong, A. Jiang, D. Ke, Q. Xu, D. Zhu, M. Bortolotti, M.J. Reece, C. Hu,
42 S. Grasso, High entropy $\text{Sr}((\text{Zr}_{0.94}\text{Y}_{0.06})_{0.2}\text{Sn}_{0.2}\text{Ti}_{0.2}\text{Hf}_{0.2}\text{Mn}_{0.2})\text{O}_{3-x}$ perovskite synthesis
43 by reactive spark plasma sintering, *J. Asian Ceram. Soc.* 0 (2019) 1–6.
44
45 doi:10.1080/21870764.2019.1595931.
46
47
48
49
50
51
52 [15] J. Gild, Y. Zhang, T. Harrington, S. Jiang, T. Hu, M.C. Quinn, W.M. Mellor, N. Zhou, K.
53 Vecchio, J. Luo, High-Entropy Metal Diborides: A New Class of High-Entropy Materials
54 and a New Type of Ultrahigh Temperature Ceramics, *Sci. Rep.* 6 (2016) 2–11.
55
56 doi:10.1038/srep37946.
57
58
59
60
61
62
63
64
65

- 1
2
3
4
5
6
7
8
9
10
11
12
13
14
15
16
17
18
19
20
21
22
23
24
25
26
27
28
29
30
31
32
33
34
35
36
37
38
39
40
41
42
43
44
45
46
47
48
49
50
51
52
53
54
55
56
57
58
59
60
61
62
63
64
65
- [16] P.H. Mayrhofer, A. Kirnbauer, P. Ertelthaler, C.M. Koller, High-entropy ceramic thin films; A case study on transition metal diborides, *Scr. Mater.* 149 (2018) 93–97.
doi:10.1016/j.scriptamat.2018.02.008.
- [17] G. Tallarita, R. Licheri, S. Garroni, R. Orrù, G. Cao, Novel processing route for the fabrication of bulk high-entropy metal diborides, *Scr. Mater.* 158 (2019) 100–104.
doi:10.1016/j.scriptamat.2018.08.039.
- [18] Y. Zhang, Z.-B. Jiang, S.-K. Sun, W.-M. Guo, Q.-S. Chen, J.-X. Qiu, K. Plucknett, H.-T. Lin, Microstructure and mechanical properties of high-entropy borides derived from boro/carbothermal reduction, *J. Eur. Ceram. Soc.* (2019) 0–1.
doi:10.1016/j.jeurceramsoc.2019.05.017.
- [19] L. Feng, W.G. Fahrenholtz, G.E. Hilmas, Two-step synthesis process for high-entropy diboride powders, *J. Am. Ceram. Soc.* (2019) jace.16801. doi:10.1111/jace.16801.
- [20] J. Dusza, P. Švec, V. Girman, R. Sedlák, E.G. Castle, T. Csanádi, A. Kovalčíková, M.J. Reece, Microstructure of (Hf-Ta-Zr-Nb)C high-entropy carbide at micro and nano/atomic level, *J. Eur. Ceram. Soc.* 38 (2018) 4303–4307. doi:10.1016/j.jeurceramsoc.2018.05.006.
- [21] E. Castle, T. Csanádi, S. Grasso, J. Dusza, M. Reece, Processing and Properties of High-Entropy Ultra-High Temperature Carbides, *Sci. Rep.* 8 (2018) 1–12. doi:10.1038/s41598-018-26827-1.
- [22] X. Yan, L. Constantin, Y. Lu, J.F. Silvain, M. Nastasi, B. Cui, (Hf_{0.2} Zr_{0.2} Ta_{0.2} Nb_{0.2} Ti_{0.2})C high-entropy ceramics with low thermal conductivity, *J. Am. Ceram. Soc.* 101 (2018) 4486–4491. doi:10.1111/jace.15779.
- [23] P. Sarker, T. Harrington, C. Toher, C. Oses, M. Samiee, J.P. Maria, D.W. Brenner, K.S. Vecchio, S. Curtarolo, High-entropy high-hardness metal carbides discovered by entropy

descriptors, *Nat. Commun.* 9 (2018) 1–10. doi:10.1038/s41467-018-07160-7.

- 1
2
3 [24] J. Gild, J. Braun, K. Kaufmann, E. Marin, T. Harrington, P. Hopkins, K. Vecchio, J. Luo, A
4 high-entropy silicide: $(\text{Mo}_{0.2}\text{Nb}_{0.2}\text{Ta}_{0.2}\text{Ti}_{0.2}\text{W}_{0.2})\text{Si}_2$, *J. Mater.* (2019).
5
6 doi:10.1016/j.jmat.2019.03.002.
7
8
9
10
11 [25] Z. Zhang, S. Fu, F. Aversano, M. Bortolotti, H. Zhang, C. Hu, S. Grasso, Arc melting: a
12 novel method to prepare homogeneous solid solutions of transition metal carbides (Zr, Ta,
13 Hf), *Ceram. Int.* 45 (2019) 9316–9319. doi:10.1016/j.ceramint.2019.01.238.
14
15
16
17
18
19 [26] A.R. Denton, N.W. Ashcroft, Vegard's law, *Phys. Rev. A.* 43 (1991).
20
21 doi:https://doi.org/10.1103/PhysRevA.43.3161.
22
23
24
25 [27] B. Post, F.W. Glaser, D. Moskowitz, Transition metal diborides, *Acta Metall.* 2 (1954) 20–
26
27 25. doi:10.1016/0001-6160(54)90090-5.
28
29
30
31 [28] H. Biloni, B. Chalmers, Origin of the equiaxed zone in small ingots, *J. Mater. Sci.* 3 (1968)
32
33 139–149. doi:10.1007/BF00585481.
34
35
36
37 [29] G.S. Cole, Inhomogeneities and their control via solidification, *Metall. Trans.* 2 (1971) 357–
38
39 370. doi:10.1007/BF02663323.
40
41
42
43 [30] S. Otani, T. Aizawa, N. Kieda, Solid solution ranges of zirconium diboride with other
44 refractory diborides: HfB_2 , TiB_2 , TaB_2 , NbB_2 , VB_2 and CrB_2 , *J. Alloys Compd.* 475 (2009)
45
46 273–275. doi:10.1016/j.jallcom.2008.08.023.
47
48
49
50
51 [31] K. Sangwal, Review: Indentation size effect, indentation cracks and microhardness
52 measurement of brittle crystalline solids - some basic concepts and trends, *Cryst. Res.*
53
54
55
56
57
58
59 [32] A. Krell, A new look at grain size and load effects in the hardness of ceramics, *Mater. Sci.*
60
61
62
63
64
65

Eng. A. 245 (1998) 277–284. doi:10.1016/S0921-5093(97)00724-7.

1
2
3 [33] S. Wang, X. Yu, J. Zhang, Y. Zhang, L. Wang, K. Leinenweber, H. Xu, D. Popov, C. Park,
4
5 W. Yang, D. He, Y. Zhao, Crystal structures, elastic properties, and hardness of high-
6
7 pressure synthesized CrB₂ and CrB₄, J. Superhard Mater. 36 (2014) 279–287.
8
9 doi:10.3103/S1063457614040066.
10

11
12
13 [34] J.R. Cahoon, Modified “hole” theory for solute impurity diffusion in liquid metals, Metall.
14
15 Mater. Trans. A Phys. Metall. Mater. Sci. 28 A (1997) 583–593. doi:10.1007/s11661-997-
16
17 0044-3.
18
19
20
21
22
23
24
25
26
27
28
29
30
31
32
33
34
35
36
37
38
39
40
41
42
43
44
45
46
47
48
49
50
51
52
53
54
55
56
57
58
59
60
61
62
63
64
65